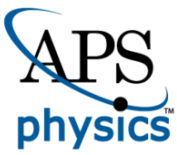

Thermoelectric transport in thin films of three-dimensional topological insulators

R. Ma, L. Sheng, M. Liu, and D. N. Sheng

Phys. Rev. B **87**, 115304 — Published 8 March 2013

DOI: 10.1103/PhysRevB.87.115304

Thermoelectric transport in thin films of three-dimensional topological insulators

R. Ma[1],* L. Sheng[2],† M. Liu[3], and D. N. Sheng[4]
[1] *School of Physics and Optoelectronic Engineering, Nanjing University of Information Science and Technology, Nanjing 210044, China*
[2] *National Laboratory of Solid State Microstructures and Department of Physics, Nanjing University, Nanjing 210093, China*
[3] *Department of Physics, Southeast University, Nanjing 210096, China*
[4] *Department of Physics and Astronomy, California State University, Northridge, California 91330, USA*

We numerically study the thermoelectric transport properties based on the Haldane model of three-dimensional topological insulator (3DTI) thin film in the presence of an exchange field g and a hybridization gap Δ. The thermoelectric coefficients exhibit rich behaviors as a consequence of the interplay between g and Δ in the 3DTI thin film. For $\Delta = 0$ but $g \neq 0$, the transverse thermoelectric conductivity α_{xy} saturates to a universal value $1.38k_Be/h$ at the center of each Landau level (LL) in the high temperature regime, and displays a linear temperature dependence at low temperatures. The semiclassical Mott relation is found to remain valid at low temperatures. If $g = 0$ but $\Delta \neq 0$, the thermoelectric coefficients are consistent with those of a band insulator. For both $g \neq 0$ and $\Delta \neq 0$, α_{xy} saturates to a universal value $0.69k_Be/h$ at the center of each LL in the high temperature regime. We attribute this behavior to the split of all the LLs, caused by the simultaneous presence of nonzero g and Δ, which lifts the degeneracies between Dirac surface states.

PACS numbers: 73.50.-h; 72.10.-d; 73.50.Lw, 73.43.Cd

I. INTRODUCTION

The field of topological insulators (TI) has attracted much attention due to its fundamental importance and potential application [1–4]. Unlike normal insulators, the TI has energy gap in the bulk and accommodates gapless edge/surface states which are protected by time-reversal symmetry. The existence of surface states in three-dimensional (3D) topological insulators, such as Bi_2Se_3 and Bi_2Te_3, have been theoretically predicted and experimentally observed[5–8]. The surface states of the TI resemble the low-energy Dirac fermions of graphene but here with only one Dirac valley on each surface with no spin degeneracy, in contrast to a four-fold degeneracy from valley and spin in graphene. This implies the expected topological robustness in 3DTI[9–11]. The metallic nature of the surface states is ensured by the nontrivial Berry phase at the Dirac point, which cannot be eliminated by scattering of weak nonmagnetic disorder. These unique properties of TIs can also be employed to make very efficient thermoelectrics[12–15]. Experimentally, the enhancement of the thermopower in Bi_2Se_3 has been observed by Qu *et al.*[15], which may be related to the dominate contributions from surface states at low temperatures[12,13].

When a perpendicular magnetic field B_0 is applied to the film, the surface states of a 3DTI are quantized into Landau levels (LLs). These LLs have the same quantization form as the Haldane model[16],

$$E_{\tau_z,n} = \mathrm{sgn}(n)\sqrt{w_1^2|n| + \left(\frac{\Delta}{2} + g\tau_z\right)^2}, \qquad (1)$$

for nonzero integer n, and

$$E_{\tau_z,0} = [g + (\Delta/2)\tau_z]\mathrm{sgn}(eB_0)\ , \qquad (2)$$

for $n = 0$. Here, g and Δ are the Zeeman energy and the hybridization gap, respectively[17]. $\tau_z = \pm 1$ representing two Dirac valleys, and $w_1 = \sqrt{2|eB_0|}v_F$ is the width of the $\nu = 1$ Hall plateau at $g = \Delta = 0$. When both g and Δ vanish, Eqs. (1) and (2) reduce to the standard LLs for massless Dirac fermions, which are additionally degenerate for $\tau_z = \pm 1$, that is, $E_{+,n} = E_{-,n}$. Here, Zeeman energy g plays the role of the staggered fluxes in the Haldane model, and the hybridization gap Δ is equivalent to the alternating on-site energies on A and B sublattices. In the previous work[17], the quantum Hall effect (QHE) of 3DTI thin film has been investigated in the presence of g and Δ. A peculiar phase diagram for the QHE is obtained driven by the competition between g and Δ, which is quite different from these either in traditional QHE or in graphene electron systems. The quantization rule of the Hall conductivity varies with nonzero g or/and Δ, which can shift the relative positions of the LLs and cause the LLs to split. Owing to these rich phase diagram for the QHE, the 3DTI thin film is expected to exhibit novel thermoelectric transport properties. However, theoretical studies of the thermoelectric transport properties of 3DTI thin film are limited, compared with those of graphene systems[18,19]. In particular, a careful examination of the thermoelectric transport properties has not been done so far in the presence of g and Δ. Such theoretical studies will provide theoretical understanding and guidance to the experimental research of the thermoelectric transport in such systems.

In this paper, we carry out a numerical study of the thermoelectric transport properties in 3DTI film in the presence of the finite Zeeman energy g and hybridization gap Δ. The effects of disorder and thermal activation on the broadening of LLs are considered. For $\Delta = 0$ but $g \neq 0$, the thermoelectric coefficients exhibit unique characteristics different from those of graphene. The po-

sitions of all the peaks for the transverse thermoelectric conductivity α_{xy} shift with nonzero g due to the shift of the positions of all the LLs. In the high temperature regime, the transverse thermoelectric conductivity α_{xy} saturates to a universal value $1.38k_Be/h$ at the center of each LL, and displays a linear temperature dependence at low temperatures. For $g = 0$ but $\Delta \neq 0$, the thermoelectric coefficients are consistent with those of a band insulator. Around zero energy, α_{xy} exhibits a pronounced valley with $\alpha_{xy} = 0$ at low temperatures. Both thermopower and Nernst signal display very large peaks at high temperatures. We show that these features are associated with a band insulator, due to the opening of a sizable gap between the valence and conductance bands. For both $g \neq 0$ and $\Delta \neq 0$, α_{xy} saturates to a universal value $0.69k_Be/h$ at the center of each LL in the high temperature regime. We attribute this behavior to the split of all the LLs, caused by the simultaneous presence of nonzero g and Δ.

This paper is organized as follows. In Sec. II, we introduce the Haldane model Hamiltonian for the 3DTI thin film in the presence of both Zeeman energy and hybridization gap and the numerical method for transport calculations. In Sec. III, we present numerical exact diagonalization results for the thermoelectric transport properties for 3DTI thin film. The final section contains a summary.

II. MODEL AND METHODS

We assume that the surface state of a thin film of 3DTI can be effectively described as a lattice model[17] with totally L_y zigzag chains and L_x atomic sites on each zigzag chain. The size of the sample will be denoted as $N = L_x \times L_y$. In the presence of an applied magnetic field perpendicular to the film of 3DTI, the Hamiltonian for the surface states can be described as the Haldane model[16]:

$$\begin{aligned} H &= -\sum_{\langle ij\rangle} t e^{ia_{ij}} c_i^\dagger c_j - \sum_{\langle\langle ij\rangle\rangle} t_2 e^{i\phi_{ij}} c_i^\dagger c_j - \sum_{\langle\langle ij\rangle\rangle} t_2 e^{ia_{ij}} c_i^\dagger c_j \\ &+ \sum_i V_i c_i^\dagger c_i + h.c. + \sum_i w_i c_i^\dagger c_i \ , \end{aligned} \tag{3}$$

Here, $c_i^\dagger(c_i)$ is the fermion creation (annihilation) operator at site i, t (t_2) is the hopping integral between the nearest-neighbor (next-nearest-neighbor) sites i and j, and $V_i = \pm M$ is the on-site energy for sublattices A and B, respectively. $\phi_{ij} = \pm\phi$ is the hopping phase from site i to its second neighbor j, due to a staggered magnetic-flux density, where the positive sign is taken for an electron hopping along the arrows indicated in Fig.1 of Ref. 16. It has been shown[16] that the Haldane model (3) exhibits a quantized Hall conductivity $\pm e^2/h$ for $3\sqrt{3}|t_2 \sin\phi| > |M|$ and behaves as a normal insulator otherwise. Under the applied magnetic field B_0, the vector potential is introduced into Eq. (3) via an additional phase factor a_{ij}, which is determined by the magnetic flux per hexagon $\varphi = \sum_{\hexagon} a_{ij} = \frac{2\pi}{M_0}$. M_0 is an integer proportional to the strength of the applied magnetic field B_0 and the lattice constant is taken to be unity. The total flux through the sample is $\frac{N\varphi}{4\pi}$, where $N = L_xL_y/M$ is taken to be an integer to satisfy the generalized boundary conditions for the single-particle magnetic translations along the $\mathbf{x}$ and $\mathbf{y}$ directions. We choose M_0 to be commensurate with L_x or L_y so that the boundary conditions are reduced to the periodic ones for wavefunctions. We model charged impurities in substrate, randomly located in a plane at a distance d, either above or below the the 3DTI thin film sheet with a long-range Coulomb scattering potential, similar to that of graphene[20–23]. For charged impurities, $w_i = -\frac{Ze^2}{\epsilon}\sum_\alpha 1/\sqrt{(\mathbf{r}_i - \mathbf{R}_\alpha)^2 + d^2}$, where Ze is the charge carried by an impurity, ϵ is the effective background lattice dielectric constant, and $\mathbf{r}_i$ and $\mathbf{R}_\alpha$ are the planar positions of site i and impurity α, respectively. All the properties of the substrate can be absorbed into a dimensionless parameter $r_s = Ze^2/(\epsilon\hbar v_F)$, where v_F is the Fermi velocity of the electrons. $\hbar v_F = \frac{3}{2}ta$, where a is lattice constant[21]. For simplicity, in the following calculation, we fix the distance $d = 1$nm and impurity density as 1% of the total sites, and tune r_s to control the impurity scattering strength. The characteristic features of the calculated transport coefficients are insensitive to the details of the impurity scattering and choices of these parameters.

In the linear response regime, the charge current in response to an electric field or a temperature gradient can be written as $\mathbf{J} = \hat{\sigma}\mathbf{E} + \hat{\alpha}(-\nabla T)$, where $\hat{\sigma}$ and $\hat{\alpha}$ are the electrical and thermoelectric conductivity tensors, respectively. The Hall conductivity σ_{xy} can be calculated by Kubo formula and the longitudinal conductivity σ_{xx} can be obtained based on the calculation of the Thouless number[24]. We exactly diagonalize the Haldane model Hamiltonian in the presence of disorder[25]. Then the transport coefficients can be calculated using the obtained energy spectra and wave functions. In practice, we can first calculate the electrical conductivity $\sigma_{ji}(E_F)$ at zero temperature, and then use the relation[26]

$$\begin{aligned} \sigma_{ji}(E_F, T) &= \int d\epsilon\, \sigma_{ji}(\epsilon) \left(-\frac{\partial f(\epsilon)}{\partial \epsilon}\right), \\ \alpha_{ji}(E_F, T) &= \frac{-1}{eT}\int d\epsilon\, \sigma_{ji}(\epsilon)(\epsilon - E_F) \left(-\frac{\partial f(\epsilon)}{\partial \epsilon}\right), \end{aligned} \tag{4}$$

to obtain the electrical and thermoelectric conductivity at finite temperature. Here, $f(x) = 1/[e^{(x-E_F)/k_BT} + 1]$ is the Fermi distribution function. At low temperatures, the second equation can be approximated as

$$\alpha_{ji}(E_F, T) = -\frac{\pi^2 k_B^2 T}{3e} \left.\frac{d\sigma_{ji}(\epsilon, T)}{d\epsilon}\right|_{\epsilon = E_F}, \tag{5}$$

which is the semiclassical Mott relation[26,27]. The thermopower and Nernst signal can be calculated subse-

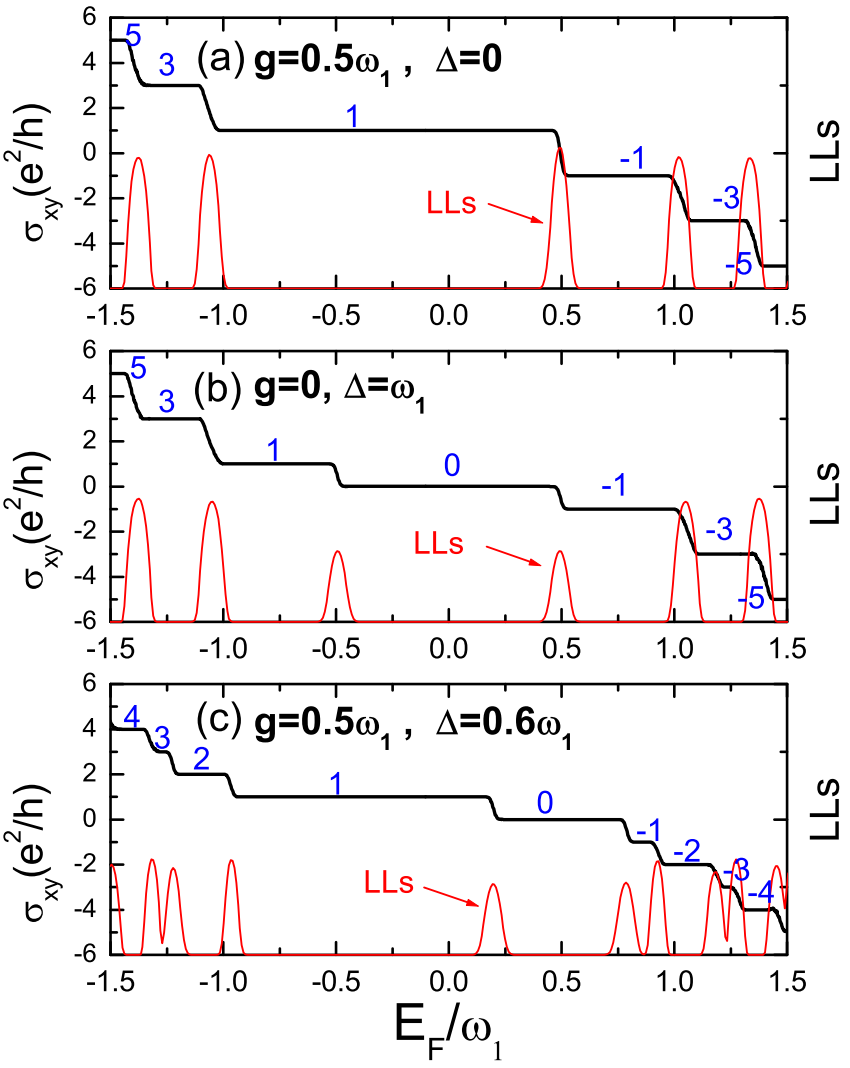

FIG. 1: (color online). Calculated Hall conductivity σ_{xy} in units of e^2/h as a function of the Fermi energy at zero temperature for (a)$g = 0.5\omega_1$ and $\Delta = 0$, (b)$g = 0$ and $\Delta = \omega_1$, (c)$g = 0.5\omega_1$ and $\Delta = 0.6\omega_1$. The system size is taken to be $N = 96 \times 48$, magnetic flux $\varphi = 2\pi/48$, and disorder strength $r_s = 0.3$ (we consider uniformly distributed positive and negative charged impurities within this strength).

quently from[28,29]

$$S_{xx} = \frac{E_x}{\nabla_x T} = \rho_{xx}\alpha_{xx} - \rho_{yx}\alpha_{yx},$$
$$S_{xy} = \frac{E_y}{\nabla_x T} = \rho_{xx}\alpha_{yx} + \rho_{yx}\alpha_{xx}. \quad (6)$$

III. THERMOELECTRIC TRANSPORT OF 3DTI THIN FILM

We start from numerically diagonalizing the Hamiltonian based on the Haldane model in the presence of disorder scattering. We first show the Hall conductivities for some different values of g and Δ at zero temperature. The three parameters we used are (1)$g = 0.5\omega_1$ and $\Delta = 0$; (2)$g = 0$ and $\Delta = \omega_1$; (3)$g = 0.5\omega_1$ and $\Delta = 0.6\omega_1$, and their corresponding Hall conductivities are shown in Fig.1, corresponding to three different quantization rules. As shown from Fig.1(a), we can see that for $g = 0.5\omega_1$ and $\Delta = 0$, there is no LL near $E_F = 0$ and the positions of all the LLs shift to both sides due to a nonzero g. All the LLs are still degenerate for $\tau_z = \pm 1$, so that the Hall conductivity remains to be odd-integer quantized $\sigma_{xy} = (2\ell + 1)\frac{e^2}{h}$ with ℓ being an integer. For $g = 0$ and $\Delta = \omega_1$, there is a splitting of the $n = 0$ LL, yielding a new plateau with $\sigma_{xy} = 0$, in addition to

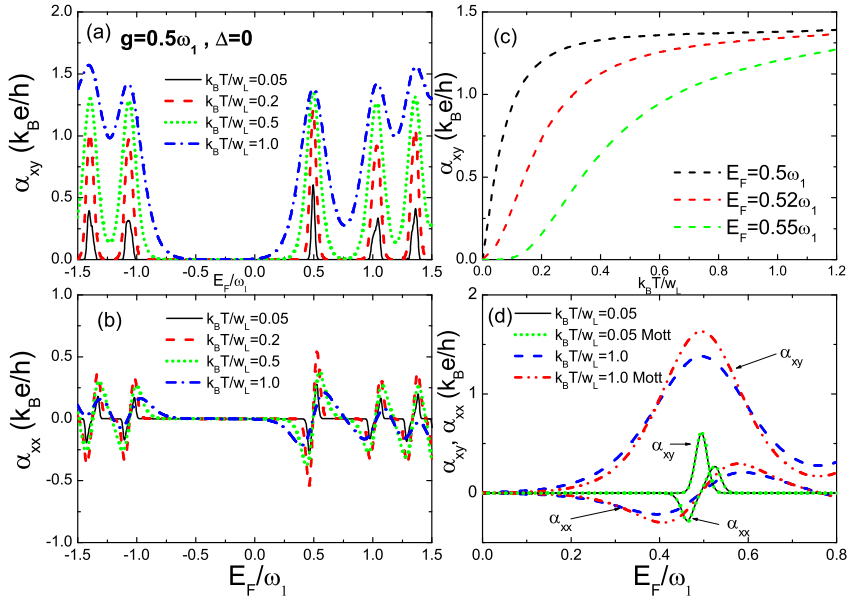

FIG. 2: (color online). Thermoelectric conductivities at finite temperatures for $g = 0.5\omega_1$ and $\Delta = 0$. (a)-(b) $\alpha_{xy}(E_F, T)$ and $\alpha_{xx}(E_F, T)$ as functions of the Fermi energy at different temperatures. (c) The temperature dependence of $\alpha_{xy}(E_F, T)$ for certain fixed Fermi energies. (d) The comparison of results from numerical calculations and from the generalized Mott relation at two characteristic temperatures, $k_BT/W_L = 0.05$ and $k_BT/W_L = 1.0$. Here $W_L/\omega_1 = 0.0612$. The system size is taken to be $N = 96 \times 48$, magnetic flux $\varphi = 2\pi/48$, and disorder strength $r_s = 0.3$.

the original odd-integer plateaus, as shown in Fig.1(b). For $g = 0.5\omega_1$ and $\Delta = 0.6\omega_1$, the simultaneous presence of nonzero g and Δ causes splitting of the degenerating LLs due to the lifting of the degeneracy between different Dirac surface states, so that all integer Hall plateaus $\sigma_{xy} = \ell\frac{e^2}{h}$ appear, as shown in Fig.1(c).

We now study the thermoelectric conductivities at finite temperatures for some different values of g and Δ. In Fig.2, we first plot the calculated thermoelectric conductivities for $g = 0.5\omega_1$ and $\Delta = 0$. As seen from Fig.2(a) and (b), the transverse thermoelectric conductivity α_{xy} displays a series of peaks, while the longitudinal thermoelectric conductivity α_{xx} oscillates and changes sign at the center of each LL. These results exhibit quite different behavior compared to those of graphene[18]. Firstly, there is no LL near $E_F = 0$ and the positions of all the peaks in α_{xy} shift to both sides due to a finite g. The peak of α_{xy} for the central ($n = 0$) LL appears at $E_F = 0.5\omega_1$. Secondly, the peak values of α_{xy} for $n = 0$ LL is smaller than that of graphene. As shown in Fig.2(b), around $E_F = 0.5\omega_1$, the peak value of α_{xx} shows different trend with increasing temperature (it first increases with T at low-temperature region, and then it decreases with T at high temperatures). This is due to the competition between $\frac{\pi^2 k_B^2 T}{3e}$ and $\frac{d\sigma_{ji}(\epsilon,T)}{d\epsilon}$ of Eq.(5). The peak value of α_{xx} could either increase or decrease depending on the relative magnitudes of these two terms. At high temperatures, $\sigma_{ji}(\epsilon, T)$ becomes smooth, and consequently α_{xx} begins to decrease. In Fig.2(c), we find that α_{xy} monotonically increases with the relative strength of temperature k_BT and the width of the central LL W_L (W_L is determined by the full-width at the half-maximum of the σ_{xx} peak). When $k_BT \ll W_L$, α_{xy} shows linear temperature dependence, indicating that there is a small energy range where extended states dominate, and the transport falls into the semi-classical Drude-Zener regime. When k_BT becomes comparable to or greater than W_L, the α_{xy} for all the LLs saturates to a constant value $1.38k_Be/h$. This matches exactly the universal value $(\ln 2)k_Be/h$ predicted for the conventional IQHE systems in the case where thermal activation dominates[26,27], with an additional degeneracy factor 2. The saturated value of α_{xy} is exactly half of that of graphene due to the lack of spin degeneracy in such a system with strong spin-orbit coupling.

To examine the validity of the semiclassical Mott relation, we compare the above results with those calculated from Eq.(5), as shown in Fig.2(d). The Mott relation is a low-temperature approximation and predicts that the thermoelectric conductivities have linear temperature dependence. This is in agreement with our low-temperature results, which proves that the semiclassical Mott relation is asymptotically valid in Landau-quantized systems, as suggested in Ref. 26.

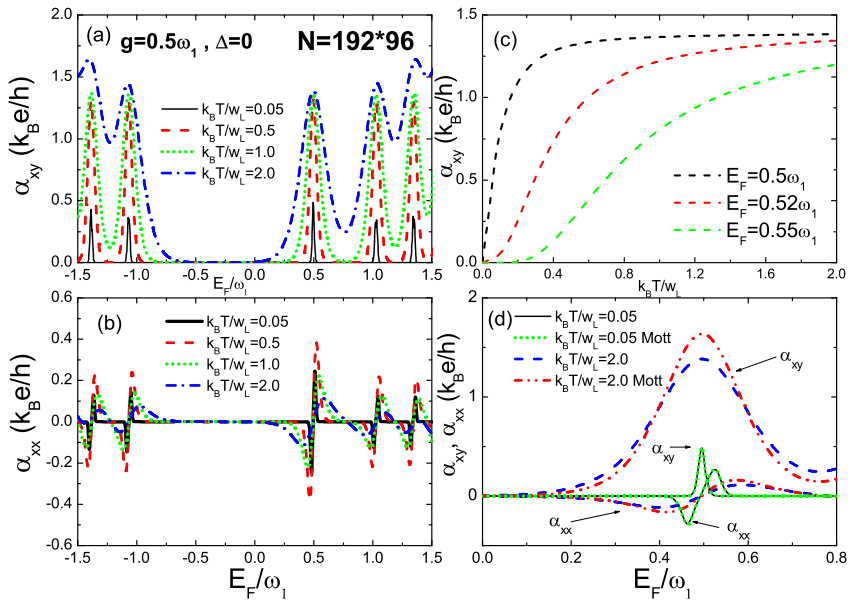

FIG. 3: (color online). Thermoelectric conductivities for $g = 0.5\omega_1$ and $\Delta = 0$ with a larger system size $N = 192 \times 96$. (a)-(b) $\alpha_{xy}(E_F, T)$ and $\alpha_{xx}(E_F, T)$ as functions of the Fermi energy at different temperatures. (c) The temperature dependence of $\alpha_{xy}(E_F, T)$ for certain fixed Fermi energies. (d) The comparison of results from numerical calculations and from the generalized Mott relation at two characteristic temperatures, $k_BT/W_L = 0.05$ and $k_BT/W_L = 2.0$. Here $W_L/\omega_1 = 0.0296$. The other parameters are chosen to be the same as in Fig.2.

We also study the thermoelectric conductivities for different system size and magnetic field in the presence of disorder. In Fig.3, we show the thermoelectric conductivities at a larger system size $N = 192 \times 96$, and the other parameters are chosen to be the same as in Fig.2. As we can see that, all the results for α_{xy} and α_{xx} remain unchanged.

In Fig.4, we show the thermoelectric conductivities at a relatively strong magnetic flux $\varphi = 2\pi/24$ for system size $N = 96 \times 48$ and disorder strengths $r_s = 0.3$. These results are qualitatively similar to those found in the weaker magnetic field case in Fig.2, while the gap between the peaks of α_{xy} is increased due to the increase of the LL gap. So, we can conclude that the characteristic features of thermoelectric conductivities are insensitive to either the magnetic field strength or the system size.

We finally focus on the disorder effect on the thermoelectric conductivities. In Fig.5, the transverse thermoelectric conductivity α_{xy} with three different disorder strengths $r_s = 0.3, 0.9$ and 1.1 are shown for system size $N = 96 \times 48$ and magnetic flux $\varphi = 2\pi/48$. In Fig.5(a), the calculated α_{xy} at a weaker disorder strength $r_s = 0.3$ are plotted. α_{xy} displays a series of peaks at the center of each LL. As seen from Fig.5(b) and (c), the width of the peak in α_{xy} increases with the increase of the disorder strength. At $r_s = 1.1$, the peaks of α_{xy} for the $n = 0$ LL remain well defined, however, other peaks for high LLs have already disappeared. The most robust peak at the $n = 0$ LL eventually disappears around $r_s \sim 1.5$, which is driven by the merging of states with opposite Chern numbers at strong disorder[32].

In Fig.6, we show the results of α_{xx} and α_{xy} for $g = 0$ and $\Delta = \omega_1$. The particle-hole symmetry is recovered in this case, however, we see that α_{xy} displays a pronounced valley, in striking contrast to that of graphene with a peak at the particle-hole symmetric point $E_F = 0$. This behavior can be understood as due to the split of the degeneracy between Dirac surface states in the $n = 0$ LL, caused by nonzero Δ. α_{xx} oscillates and changes sign around the center of each split LL. In Fig.6(c), we also compare the above results with those calculated from the semiclassical Mott relation using Eq.(5). The Mott relation is found to remain valid at low temperatures.

In Fig.7, we show the results of α_{xx} and α_{xy} for $g = 0.5\omega_1$ and $\Delta = 0.6\omega_1$. As we can see, α_{xy} displays a series of peaks, while α_{xx} oscillates and changes sign at the center of each LL. These results are qualitatively similar to those found in 3DTI case in Fig.2, but some obvious differences exist. Firstly, the position of the peak in α_{xy} for the $n = 0$ LL shift, and the peak value is smaller than that of Fig.2. Secondly, at low temperature, α_{xy} splits in the higher LLs, which can be understood as due to the presence of all integer Hall plateaus. In Fig.7(c), we find that, when k_BT becomes comparable to or greater than W_L, the α_{xy} for all the LLs saturates to a constant value $0.69k_Be/h$. The saturated value of

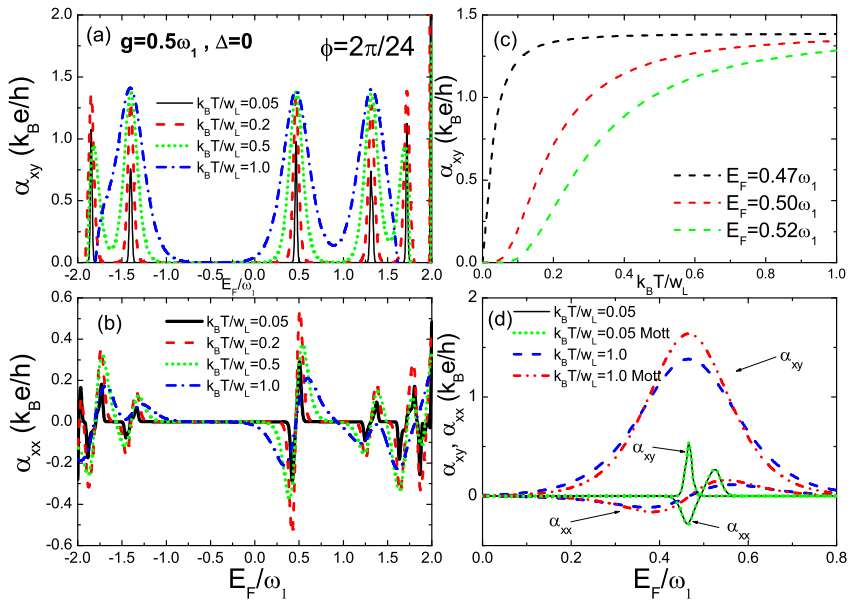

FIG. 4: (color online). Thermoelectric conductivities for $g = 0.5\omega_1$ and $\Delta = 0$ with a stronger magnetic field $\varphi = 2\pi/24$. (a)-(b) $\alpha_{xy}(E_F, T)$ and $\alpha_{xx}(E_F, T)$ as functions of the Fermi energy at different temperatures. (c) The temperature dependence of $\alpha_{xy}(E_F, T)$ for certain fixed Fermi energies. (d) The comparison of results from numerical calculations and from the generalized Mott relation at two characteristic temperatures, $k_BT/W_L = 0.05$ and $k_BT/W_L = 1.0$. Here $W_L/\omega_1 = 0.0822$. The other parameters are chosen to be the same as in Fig.2.

α_{xy} can be understood as the lifting the degeneracy of all the LLs due to the simultaneous presence of nonzero g and Δ. In Fig.7(d), we also compare the above results with those calculated from the semiclassical Mott relation using Eq.(5). The Mott relation is also found to remain valid only at low temperatures.

We further calculate the thermopower S_{xx} and the Nernst signal S_{xy} using Eq. (6), which can be directly determined in experiments by measuring the responsive electric fields. In Fig.8(a)-(b), we show the results of S_{xx} and S_{xy} for $g = 0.5\omega_1$ and $\Delta = 0$. As we can see, S_{xy} (S_{xx}) has a peak at the $n = 0$ LL (the other LLs), and changes sign near the other LLs (the $n = 0$ LL). At $E_F = 0.5\omega_1$ energy point, both ρ_{xy} and α_{xx} vanish, leading to a vanishing S_{xx}. Around $E_F = 0.5\omega_1$, because $\rho_{xx}\alpha_{xx}$ and $\rho_{xy}\alpha_{xy}$ have opposite signs, depending on their relative magnitudes, S_{xx} could either increases or decreases when E_F is increased passing the $E_F = 0.5\omega_1$. In our calculation, S_{xx} is always dominated by $\rho_{xy}\alpha_{xy}$, and consequently S_{xx} increases to positive value as E_F passing the $E_F = 0.5\omega_1$. At low temperature, the peak value of S_{xx} near zero energy is $\pm 0.33 k_B/e$ ($\pm 28.44\mu V/K$) at $k_BT = 0.2W_L$. With the increase of temperature, the peak height increases to $\pm 2.67 k_B/e$ ($\pm 230.07\mu V/K$) at $k_BT = 1.0W_L$. On the other hand, S_{xy} has a peak structure around $E_F = 0.5\omega_1$, which is dominated by $\rho_{xx}\alpha_{xy}$. We find that the peak height is $5.69 k_B/e$ ($490.31\mu V/K$) at $k_BT = 1.0W_L$.

In Fig.8(c)-(d), we show the calculated S_{xx} and S_{xy} for $g = 0$ and $\Delta = \omega_1$. As we can see, at low temperatures, both S_{xx} and S_{xy} vanish around zero energy. This behavior can be understood as due to the opening of a sizable gap between the valence and conduction bands in a band insulator. At high temperatures, S_{xx} changes sign around zero energy. In our calculation, S_{xx} is dominated by $\rho_{xy}\alpha_{xy}$. The peak value of S_{xx} near zero energy is around $\pm 9.03 k_B/e$ ($\pm 778.12\mu V/K$) at $k_BT = 2.0W_L$. Theoretical study[30] indicates that, the large magnitude of S_{xx} is mainly a result of the energy gap. On the other hand, S_{xy} has a peak structure around zero energy, which is dominated by $\alpha_{xy}\rho_{xx}$. We find that the peak height is $14.97 k_B/e$ ($1289.96\mu V/K$) at $k_BT = 2.0W_L$, which is much larger than that of shown in Fig.8(b).

In Fig.8(e)-(f), we show the calculated S_{xx} and S_{xy} for $g = 0.5\omega_1$ and $\Delta = 0.6\omega_1$. As we can see, at low temperatures, both S_{xx} and S_{xy} vanish around $E_F = 0.5\omega_1$. This behavior can be understood as due to the presence of the energy gap. At high temperatures, S_{xx} changes sign around $E_F = 0.5\omega_1$. In our calculation, S_{xx} is dominated by $\rho_{xy}\alpha_{xy}$. The peak value of S_{xx} near $E_F = 0.5\omega_1$ is around $\pm 4.51 k_B/e$ ($\pm 388.63\mu V/K$) at $k_BT = 1.0W_L$, which is much larger than that of graphene. We attribute that the large magnitude of S_{xx} is mainly a result of the energy gap near the $E_F = 0.5\omega_1$. On the other hand, at high temperatures, S_{xy} has a peak structure around $E_F = 0.5\omega_1$, which is dominated by $\alpha_{xy}\rho_{xx}$.

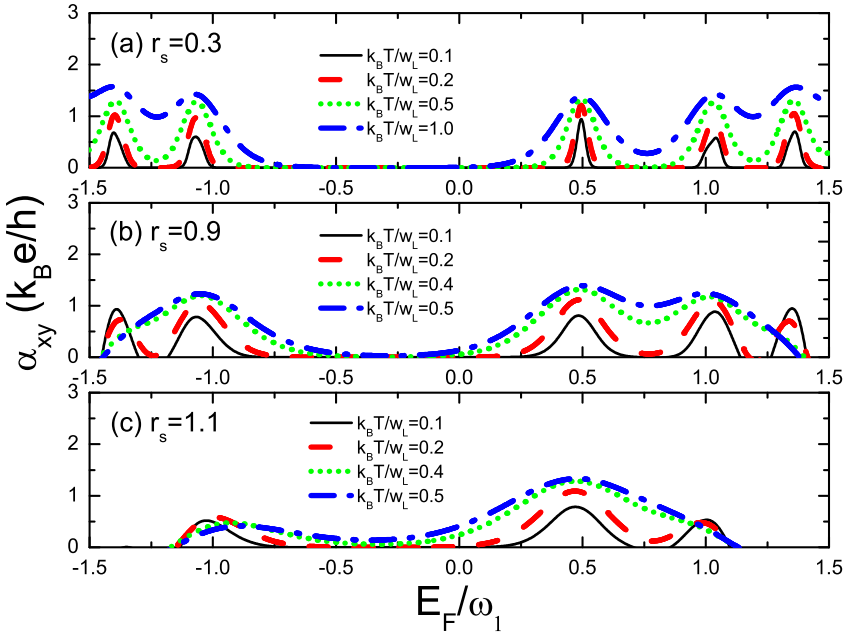

FIG. 5: (color online). The transverse thermoelectric conductivities α_{xy} for $g = 0.5\omega_1$ and $\Delta = 0$ at three different disorder strength. (a)$r_s = 0.3$, (b)$r_s = 0.9$ and (c)$r_s = 1.1$. Here the width of the central LL W_L are equal to $W_L/\omega_1 = 0.0612, 0.215$, and 0.3106, respectively. The other parameters are chosen to be the same as in Fig.2.

IV. SUMMARY

In summary, we have numerically investigated the thermoelectric transport properties based on the Haldane model of 3DTI thin film in the presence of Zeeman energy g and hybridization gap Δ. By tuning g and Δ, the thermoelectric coefficients exhibit rich features different from those of graphene system. For $\Delta = 0$ but $g \neq 0$, all the LLs are shifted away from $E_F = 0$ due to a finite g. In the high temperature regime, the transverse thermoelectric conductivity α_{xy} saturates to a universal value $1.38k_Be/h$ at the center of each LL, and displays a linear temperature dependence at low temperatures. The saturated value of α_{xy} is exactly half of that of graphene due to the lack of spin degeneracy in such a system with strong spin-orbit coupling. The Nernst signal displays a peak at the central LL with a height of the order of k_B/e, and changes sign near other LLs, while the thermopower behaves in an opposite manner. The semiclassical Mott relation is found to remain valid at low temperatures. If $g = 0$ but $\Delta \neq 0$, the thermoelectric coefficients are consistent with those of a band insulator. Around zero energy, α_{xy} exhibits a pronounced valley with $\alpha_{xy} = 0$, in striking contrast to that of graphene with a peak at the particle-hole symmetric point $E_F = 0$. This behavior can be understood as due to the split of the degeneracy in the $n = 0$ LL, caused by nonzero Δ. Both thermopower and Nernst signal display very large peaks at high temperatures. We show that these features are associated with a band insulator, due to the opening of a sizable gap between the valence and conductance bands. For both $g \neq 0$ and $\Delta \neq 0$, α_{xy} saturates to a universal value $0.69k_Be/h$ at the center of each LL in the high temperature regime. We attribute this behavior to the split of all the LLs, caused by the simultaneous presence of nonzero g and Δ, which lifts the degeneracies between Dirac surface states.

Acknowledgments

We would like to thank Huichao Li for stimulating discussion. This work is supported by the National Natural Science Foundation of China (NSFC) Grant No. 11104146 (R.M.), the NSFC Grant No. 11074110, the National Basic Research Program of China under Grant No. 2009CB929504 (L.S.). We also thank the US NSF Grants No. DMR-0906816 and No. DMR-1205734 (D.N.S.), and Princeton MRSEC Grant No. DMR-0819860.

APPENDIX

The Hall conductivity σ_{xy} at zero temperature can be

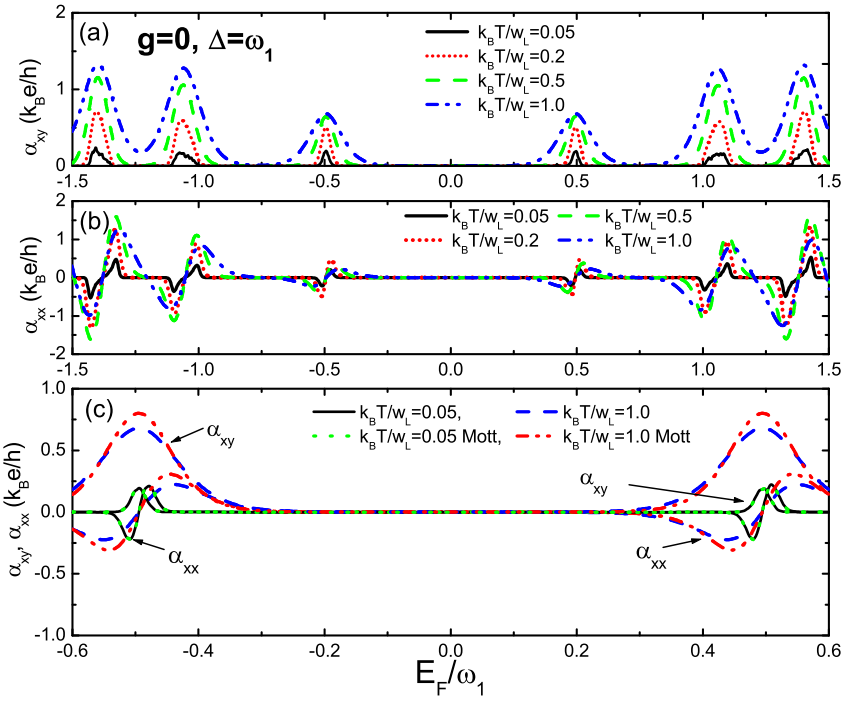

FIG. 6: (color online). Thermoelectric conductivities at finite temperatures for $g = 0$ and $\Delta = \omega_1$. (a)-(b) $\alpha_{xy}(E_F, T)$ and $\alpha_{xx}(E_F, T)$ as functions of the Fermi energy at different temperatures. (c) Compares the results from numerical calculations and from the generalized Mott relation at two characteristic temperatures, $k_BT/W_L = 0.05$ and $k_BT/W_L = 1.0$. Here $W_L/\omega_1 = 0.034$. The system size is taken to be $N = 96 \times 48$, magnetic flux $\varphi = 2\pi/48$, and disorder strength $r_s = 0.3$.

calculated by using the Kubo formula

$$\sigma_{xy} = \frac{ie^2\hbar}{S} \sum_{\varepsilon_\beta < E_F < \varepsilon_\alpha} \frac{\langle \alpha \mid V_x \mid \beta \rangle \langle \beta \mid V_y \mid \alpha \rangle - h.c.}{(\epsilon_\alpha - \epsilon_\beta)^2},$$

Here, ϵ_α, ϵ_β are the eigenenergies corresponding to the eigenstates $|\alpha\rangle$, $|\beta\rangle$ of the system, which can be obtained through exact diagonalization of the Haldane model Hamiltonian. S is the area of the sample, V_x and V_y are the velocity operators. With tuning chemical potential E_F, a series of integer-quantized plateaus of σ_{xy} appear, each one corresponding to E_F moving in the gaps between two neighboring Landau Levels (LLs).

The longitudinal conductivity σ_{xx} at zero temperature can be obtained based on the calculation of the Thouless number. The Thouless number g is calculated by using the following formula[31]

$$g = \frac{\Delta E}{dE/dN}$$

Here, ΔE is the geometric mean of the shift in the energy levels of the system caused by replacing periodic by antiperiodic boundary conditions, and dE/dN is the mean spacing of the energy levels. The Thouless number g is proportional to the longitudinal conductivity σ_{xx}.

Once we obtain the electrical conductivity σ_{xy} and σ_{xx} at zero temperature, and then we can use Eq.(4) to obtain the electrical and thermoelectric conductivity at finite temperature.

* Electronic address: njrma@hotmail.com
† Electronic address: shengli@nju.edu.cn

[1] X. L. Qi and S. C. Zhang, Phys. Today **63**, No.1, 33 (2010).
[2] M. Z. Hasan and C. L. Kane, Rev. Mod. Phys. **82**, 3045 (2010).
[3] J. E. Moore, Nature **464**, 194 (2010).
[4] X. L. Qi and S. C. Zhang, Rev. Mod. Phys. **83**, 1057 (2011).
[5] H. J. Zhang, C. X. Liu, X. L. Qi, X. Dai, Z. Fang, and S. C. Zhang, Nature Phys. **5**, 438 (2009).
[6] Y. Xia, D. Qian, D. Hsieh, L. Wray, A. Pal, H. Lin, A. Bansil, D. Grauer, Y. S. Hor, R. J. Cava et al., Nature Phys. **5**, 398 (2009).
[7] Y. L. Chen, J. G. Analytis, J. H. Chu, Z.K. Liu, S. K. Mo, X. L. Qi, H. J. Zhang, D. H. Lu, X. Dai, Z. Fang, S. C.

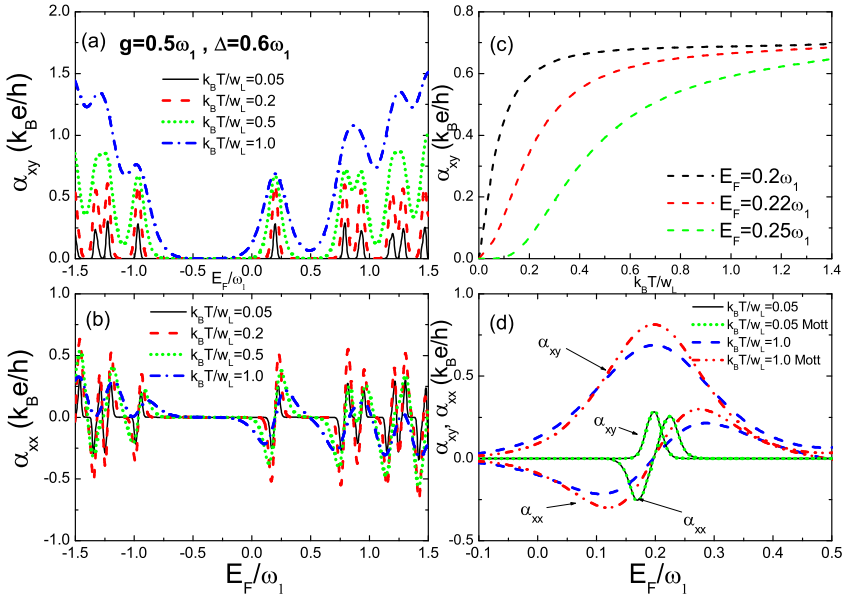

FIG. 7: (color online). Thermoelectric conductivities at finite temperatures for $g = 0.5\omega_1$ and $\Delta = 0.6\omega_1$. (a)-(b) $\alpha_{xy}(E_F, T)$ and $\alpha_{xx}(E_F, T)$ as functions of the Fermi energy at different temperatures. (c) shows the temperature dependence of $\alpha_{xy}(E_F, T)$ for certain fixed Fermi energies. (d) compares the results from numerical calculations and from the generalized Mott relation at two characteristic temperatures, $k_BT/W_L = 0.05$ and $k_BT/W_L = 1.0$. Here $W_L/\omega_1 = 0.0556$. The system size is taken to be $N = 96 \times 48$, magnetic flux $\varphi = 2\pi/48$, and disorder strength $r_s = 0.3$.

Zhang, I. R. Fisher, Z. Hussain and Z. X. Shen, Science **325**, 178 (2009).

[8] D. Hsieh, Y. Xia, D. Qian, L. Wray, J. H. Dil, F. Meier, J. Osterwalder, L. Patthey, J. G. Checkelsky, N. P. Ong, A. V. Fedorov, H. Lin, A. Bansil, D. Grauer, Y. S. Hor, R. J. Cava, and M. Z. Hasan, Nature (London) **460**, 1101 (2009).

[9] L. Fu, C. L. Kane, and E. J. Mele, Phys. Rev. Lett. **98**, 106803 (2007).

[10] J. E. Moore, and L. Balents, Phys. Rev. B **75**, 121306 (2007).

[11] R. Roy, Phys. Rev. B **79**, 195322 (2009).

[12] R. Takahashi and S. Murakami, Phys. Rev. B **81**, 161302 (2010).

[13] P. Ghaemi, R. S. K. Mong, and J. E. Moore, Phys. Rev. Lett. **105**, 166603 (2010).

[14] O. A. Tretiakov, A. Abanov, S. Murakami, and J. Sinova, Appl. Phys. Lett., **97**, 073108 (2010); O. A. Tretiakov, A. Abanov, and J. Sinova, *ibid.* **99**, 113110 (2011).

[15] D. X. Qu, Y. S. Hor, R. J. Cava and N. P. Ong, arXiv:1108.4483 (2011).

[16] F. D. M. Haldane, Phys. Rev. Lett. **61**, 2015 (1988).

[17] H. C. Li, L. Sheng, and D. Y. Xing, Phys. Rev. B **84**, 035310 (2011).

[18] L. Zhu, R. Ma, L. Sheng, M. Liu, and D. N. Sheng, Phys. Rev. Lett. **104**, 076804 (2010).

[19] R. Ma, L. Zhu, L. Sheng, M. Liu, and D. N. Sheng, Phys. Rev. B **84**, 075420 (2011).

[20] S. Das Sarma, S. Adam, E. H. Hwang and E. Rossi, Rev. Mod. Phys. **83**, 407 (2011); S. Adam and S. Das Sarma, Solid State Communications **146**, 356 (2008).

[21] N. M. R. Peres, F. Guinea, and A. H. Castro Neto, Phys. Rev. B **72**, 174406 (2005).

[22] Y. W. Tan, Y. Zhang, K. Bolotin, Y. Zhao, S. Adam, E. H. Hwang, S. Das Sarma, H. L. Stormer, and P. Kim, Phys. Rev. Lett. **99**, 246803 (2007).

[23] J. H. Chen, C. Jang, S. Adam, M. S. Fuhrer, E. D. Williams, and M. Ishigami, Nature Physics **4**, 377 (2008).

[24] R. Ma, L. Sheng, R. Shen, M. Liu and D. N. Sheng, Phys. Rev. B **80**, 205101 (2009); R. Ma, L. Zhu, L. Sheng, M. Liu, D. N. Sheng, Europhys. Lett. **87**, 17009 (2009)

[25] D. N. Sheng and Z. Y. Weng, Phys. Rev. Lett. **78**, 318 (1997).

[26] M. Jonson and S.M. Girvin, Phys. Rev. B **29**, 1939 (1984).

[27] H. Oji, J. Phys. C **17**, 3059 (1984).

[28] X. Z. Yan and C. S. Ting, Phys. Rev. B **81**, 155457 (2010).

[29] Different literatures may have a sign difference due to different conventions.

[30] L. Hao and T. K. Lee, Phys. Rev. B **81**, 165445 (2010).

[31] J. T. Edwards and D. J. Thouless, J. Phys. C **5**, 807 (1972); D. J. Thouless, Phys. Rep. 13C, 93 (1974)

[32] D. N. Sheng, L. Sheng, and Z. Y. Weng, Phys. Rev. B **73**, 233406 (2006).

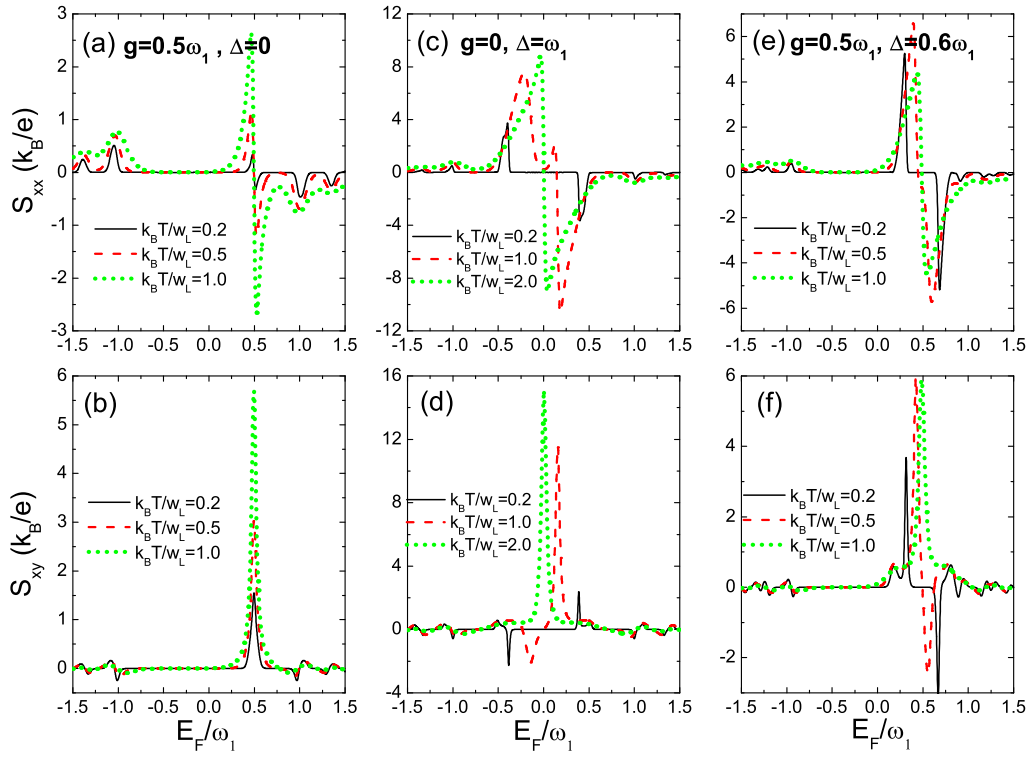

FIG. 8: (color online). The thermopower S_{xx} and the Nernst signal S_{xy} as functions of the Fermi energy for some different values of g and Δ. (a)-(b)$g = 0.5w_1$ and $\Delta = 0$, (c)-(d) $g = 0$ and $\Delta = w_1$, and (e)-(f) $g = 0.5w_1$ and $\Delta = 0.6w_1$. All parameters in this three systems are chosen to be the same as in Fig.2, Fig.6 and Fig.7, respectively.